Nucleic Acids Research, 2024, 1–14
https://doi.org/10.1093/nar/gkae311
RNA and RNA-protein complexes

Epigenetic control of adaptive or homeostatic splicing during interval-training activities

Ling Liu[1], Hai Nguyen[1], Urmi Das[1], Samuel Ogunsola[1], Jiankun Yu[1], Lei Lei[1], Matthew Kung[1], Shervin Pejhan[2], Mojgan Rastegar[2] and Jiuyong Xie[1,*]

[1]Department of Physiology & Pathophysiology, Max Rady College of Medicine, Rady Faculty of Health Sciences, University of Manitoba, Winnipeg, MB, Canada
[2]Biochemistry & Medical Genetics, Max Rady College of Medicine, Rady Faculty of Health Sciences, University of Manitoba, Winnipeg, MB, Canada

*To whom correspondence should be addressed. Tel: +1 204 975 7774; Email: xiej@umanitoba.ca

Abstract

Interval-training activities induce adaptive cellular changes without altering their fundamental identity, but the precise underlying molecular mechanisms are not fully understood. In this study, we demonstrate that interval-training depolarization (ITD) of pituitary cells triggers distinct adaptive or homeostatic splicing responses of alternative exons. This occurs while preserving the steady-state expression of the *Prolactin* and other hormone genes. The nature of these splicing responses depends on the exon's DNA methylation status, the methyl-C-binding protein MeCP2 and its associated CA-rich motif-binding hnRNP L. Interestingly, the steady expression of the *Prolactin* gene is also reliant on MeCP2, whose disruption leads to exacerbated multi-exon aberrant splicing and overexpression of the hormone gene transcripts upon ITD, similar to the observed hyperprolactinemia or activity-dependent aberrant splicing in Rett Syndrome. Therefore, epigenetic control is crucial for both adaptive and homeostatic splicing and particularly the steady expression of the *Prolactin* hormone gene during ITD. Disruption in this regulation may have significant implications for the development of progressive diseases.

Graphical abstract

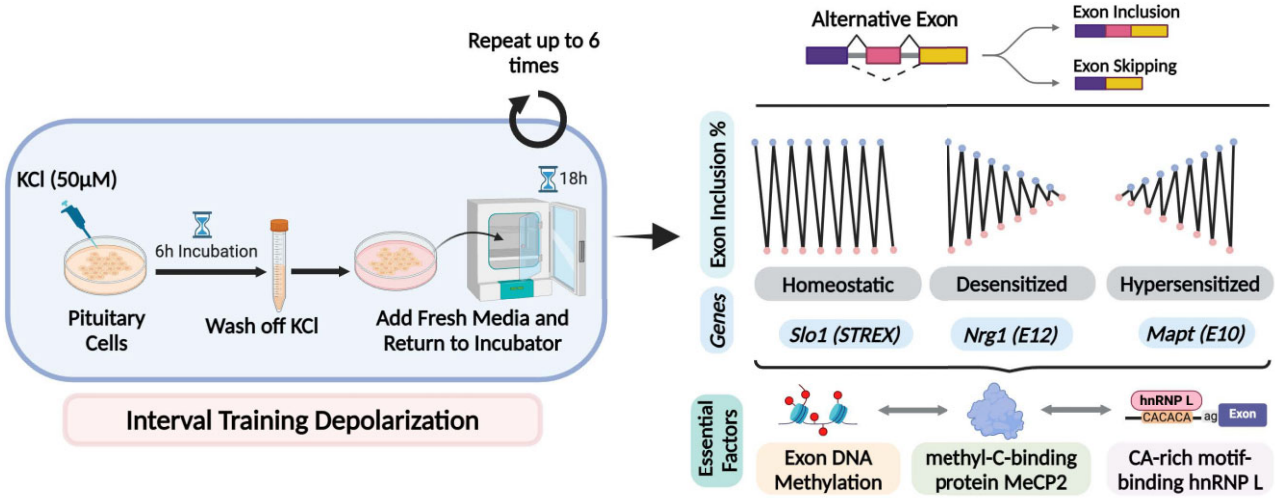

Introduction

Interval-training activities confer beneficial effects on cardiac, muscular and endocrine functions that cannot be attained through a single bout of activity (1–4). Despite this, the underlying molecular and cellular mechanisms for the adaptive as well as homeostatic responses of different genes remain to be fully elucidated. The regulation of gene expression is critical in facilitating adjustments essential for functions such as hormone synthesis (2,5,6). However, the regulation of alternative pre-mRNA splicing (7), a fundamental mechanism driving the diversification of metazoan transcriptomes and proteomes to support intricate cellular functions (8,9), remains enigmatic in the adaptation process.

We have explored how cellular activities, particularly through membrane depolarization, regulate alternative splicing in pituitary cells (10–13), where we predicted that cells

Received: February 20, 2024. **Revised:** April 3, 2024. **Editorial Decision:** April 5, 2024. **Accepted:** April 14, 2024

adapt their splicing patterns after repeated stimulation compared to initial treatments (12). This regulation has been shown to be crucial for the alternative splicing of various genes in response to chronic changes in membrane potentials, significantly affecting neuronal electrical homeostasis or synaptic formation (14–16). The regulatory mechanisms involve Ca^{++}/calmodulin-dependent protein kinase IV (CaMKIV) and downstream splicing factors such as hnRNP L/LL (10–12,17), Sam68 (15) or Nova-2 (14), depending on the target exon. Additionally, histone modifications and the methyl-DNA-binding protein MeCP2 play a key role in activity-dependent regulation, suggesting epigenetic influences (18–20). However, the role of DNA methylation in this process remains unclear.

DNA methylation is pivotal in adaptation (1,21), and generally correlates with exon inclusion in the genome/transcriptome (21), though not in all cases (22). The correlation aligns with the regulatory effects of MeCP2 and the methyl-free DNA-binding CTCF on splicing (23–25). MeCP2, which binds to specific nucleotide sequences mCAC and mCG (26), influences gene transcription and splicing (25–27). Notably, *MECP2* mutations are identified in up to 96% of typical Rett syndrome cases (28–30), a severe neurodevelopmental disorder with autistic features and often exacerbated by abnormal brain activities like epilepsy (31). In *Mecp2*-null mouse models of Rett syndrome, long genes' expression and synaptic exon splicing in the hippocampus, particularly after calcium signal-activating kainic acid treatment, are significantly impacted (19,32). Interestingly, both DNA methyltransferase DNMT3a and MeCP2 are regulated by calcium signaling: DNMT3a is recruited by CaMKIV-regulated CREMα in T lymphocytes (33,34), and MeCP2 is phosphorylated by CaMKII in hippocampal neurons (35). MeCP2 likely modulates alternative splicing through its interaction with methylated DNA and splicing factors like YB-1 (25,36). Together, DNA methylation/MeCP2 dysfunction likely plays important roles in the development of neurological diseases as many other epigenetic changes (37). However, bioinformatics analyses suggest minimal global effects of DNMTs and MeCP2 on alternative splicing (38). These inconsistencies highlight the need for further research using comprehensive methylation and splicing analyses, including direct methylation of exon DNA in splicing assays, to clarify the effects of DNA methylation and MeCP2 on splicing.

Here, we show the distinct effects of interval-training depolarization (ITD) compared to a single round of treatment on the adaptive splicing of exons in the prolactin- and growth hormone-producing pituitary cells (39). We identified a critical role of epigenetic control in both adaptive or homeostatic splicing and *Prolactin* gene expression, a dual function in adaptation while preserving cell identity.

Materials and methods

Cell culture

Rat GH_3 pituitary cells were cultured at 37°C with 5% CO_2 in Ham's F10 nutrient mixture with 10% horse serum plus 5% fetal bovine serum (FBS), and human embryonic kidney (HEK) 293T cells in DMEM with 10% FBS. Penicillin-streptomycin-glutamine solution was added to all cultures except GH_3 (without glutamine). HEK293T cells were dispersed by trypsin (0.05%, w/v)–EDTA (0.53 mM) solution during subculture.

Interval training depolarization by KCl treatments and RNA/DNA extraction

For the ITD KCl treatment group, GH_3 cultures were treated with KCl (50 mM) for 6 h, then washed and supplied with complete fresh medium, followed by incubation for 18 h, completing the 1st round (day) of the KCl treatment, which was repeated up to the 6th time (6th KCl). For the single KCl treatment group (1st KCl), cells went through the same medium change process except that KCl (50 mM) was added on the 6th day. Where applicable, DMSO or 5-aza-Cytidine (50 μM) was added to fresh culture medium 18 h before the 1st or 6th KCl-treatment. Cell density was maintained throughout the experiment by splitting them into extra dishes.

For samples for RNA-Seq only, we extracted total RNA with the GenElute™ Mammalian Total RNA Miniprep Kit (#RTN350-1KT, Sigma Aldrich, USA). For both RNA-Seq and whol-genome bisulfite sequencing (WGBS), we extracted cytoplasmic RNA for RNA-Seq and the corresponding nuclear DNA for WGBS, using our previous nucleo-cytoplasmic fractionation protocol (40,41). For RT-PCR of the non-RNA-Seq samples, cytoplasmic RNA was used.

RNA-Seq and WGBS analyses

RNA-Seq analyses were performed the same as our previous procedures (40), except that the Illumina HiSeq4000 paired-end 100-bp sequencing was used for the total RNA of non-treated (NT), 1st KCl or 6th KCl samples, and the Illumina NovaSeq 6000 S2 paired-end 100-bp sequencing was used for the cytoplasmic RNA of the 6th KCl samples with or without 24 h pre-treatment by 5-azaC (50 μM). Alternative exons, alternative transcription starts and alternative polyadenylation were identified by DEXSeq (40,42); alternative splice junctions by MATS (43); differential gene expression by edgeR (44).

For WGBS analyses, approximately 1 μg of gDNA each sample was subject to bisulfite conversion for shotgun library construction (NEB Ultra II) and Illumina HiSeqX PE150 sequencing, yielding 150-bp paired-end reads. DNA quality control, library preparation, Illumina library quality control and Illumina HiSeqX PE150 sequencing were conducted at the McGill University Génome Québec Innovation Centre (Montréal, Québec, Canada). We obtained an average of 66 ± 4 million of paired-end reads. The sequence quality was verified using FastQC (45), with the high-quality reads mapped to the rat genome assembly Rnor_6.0.84 (GH_3 samples) or mouse assembly GRCm38 (mm10, hippocampus tissue samples), using BSMAP (17,46). The DNA methylation status of individual cytosines of each exon was obtained by filtering the BSMAP output list with the genomic coordinates within the DEXSeq list of changed exons. Total DNA methylation level of an exon (mCpG or mCpH) was calculated by multiplying the average methylation ratio of CpG or CpH cytosines with the total number of mCpG or mCpH sites, respectively, in the sense strand of each exon.

For functional enrichment analysis and functional annotation of genes, we used the Database for Annotation, Visualization and Integrated Discovery (DAVID, developed at the U.S. National Institute of Allergy and Infectious Diseases, https://david.ncifcrf.gov) (47). For sequence motif

analysis, the MEME was used with default parameters (48,49). The motifs presented have the highest scores for tested data set.

Semi-quantitative RT-PCR

RT-PCR was performed based on our previous procedures (10,40). Briefly, for reverse transcription, 300 ng of cytoplasmic RNA was used in a 10 μl-reaction and incubated at 45°C for 50min. For PCR, 1μl of RT product was amplified in a 12.5 μl-reaction for 28–32 cycles. PCR products were resolved in 2–2.5% agarose gels containing ethidium bromide (EtBr), visualized under UV light and captured by a digital camera. Percentages of the splice variants were calculated based on band intensities quantified using ImageJ (National Institutes of Health).

Exon rank/numbers in the text/gels are based on the RGSC 6.0/rn6 assembly: *Slo1* STREX (exon), NM_031828.1; *Rps24* last exons, FN801636 (upper band) & NM_031112.1 (lower band); *Ehmt2* exon 9, NM_212463.1; *Dlg1* exon 20a, NM_012788.1; *Epb41l3* exon 15, NM_053927.1; Kidins220 exon 26, NM_053795.1; *Mapt* exon 6, M84156, equivalent to human *MAPT* exon 4a (NM_001123066.3, GRCh38/hg38); *Mapt* exon 7a, M84156, equivalent to human *MAPT* exon 6 (NM_001123066.3, GRCh38/hg38); *Mapt* exon 10, M84156, equivalent to human *MAPT* exon 10 (NM_001123066.3, GRCh38/hg38); *Nrg1* exon 12, NM_001271128.1; *Phldb1* exon 10, X74226. *Baiap2* exon 3, CK840478, equivalent to the mouse *Baiap2* exon 14 (ENSMUST00000106233.1, GRCm38/mm10, Figure 2).

Splicing reporter assay

Three complementary pairs of oligo inserts are listed below with different exon methylation capacities (CpG sites underlined) were synthesized using the *mBaiap2* exon 14 as a template: $(CpG)_{x3}$, $(CpG)_{x7}$ and $(GC)_{x7m}$, containing 3, 7 and 3 CpG sites, respectively, harboring the 48 bp exon (uppercases) and partial flanking introns (lowercases) with ApaI (5′-GGGCC↓C-3′) and BglII (5′-A↓GATCT-3′) restriction sites at the 5′ and 3′ ends, respectively. Complementary single-stranded oligos were denatured at 95°C, 5min and annealed at 60°C 30min before restriction digestion and ligation into the vector of the splicing reporter.

$(CpG)_{x3}$:

5′-gcgggccctgaccttgtgtttccttacagCGCGGATGTCGAAGT
GGCCAGATTTTGAGCTGCCCCTG
ACTAGAGTTAgtaagttgagatctatgc-3′

$(CpG)_{x7}$:

5′-gcgggccctgaccttgtgtttccttacagCGCGGATGTCGAAGT
GGCGCGATTTTGAGCTGCCCGCG
ACTAGAGTTAgtaagttgagatctatgc-3′

$(CpG)_{x7m}$:

5′-gcgggccctgaccttgtgtttccttacagCGCGGATGTCGAAGT
GGCCAGATTTTGAGCTGGGCCTG
ACTAGAGTTAgtaagttgagatctatgc-3′

The splicing reporter assay for the unmethylated and methylated dsDNA inserts was based on a reported procedure for transcription assay (50). Briefly, 72 μg of each insert dsDNA fragment was digested by ApaI (#ER1415, Thermo Fisher Scientific, US) and BglII (#ER0082, Thermo Fisher Scientific, US), fractionated in 1% agarose gel, excised and purified using the QIAquick Gel Extraction Kit (#28706, QIAGEN, Germany). Half of the DNA was methylated *in vitro* with the CpG methyltransferase M.SssI (M0226L, New England Biolabs, USA) using S-adenosylmethionine (SAM) as a methyl group donor, and the methylation efficiency verified by the CpG methylation-sensitive restriction enzyme BstUI (restriction site: CpG↓CpG, #R0518S, New England Biolabs, USA). The insert DNA fragments with or without methylation were ligated with the same double-digested splicing reporter vector DUP175 (12), by T4 DNA ligase (Cat. # 15224-041, Invitrogen, USA) at 14–16°C overnight. The ligated splicing reporters containing the methylated or unmethylated exons were concentrated using the QIAquick Gel Extraction Kit and co-transfected directly with the Flag-CaMKIV-dCT (CaMKIV) or –dCT-K75E (CaMKIVm) expression plasmid (12,51,52), into HEK293T cells using LipoFectamine 3000 (#L3000008, Invitrogen, USA) and incubated overnight (16–18 h) before RNA extraction.

Lentivirus transduction and gene overexpression

The lentiviruses were purchased from GeneChem. The target sequence of MeCP2 shRNA is 5′-CAGCATCTGCAAAGAGGAGAA-3′, hnRNP L shRNA is 5′-GCTATGGTGGAGTTTGATTCT-3′, and the non-targeting control is 5′-TTCTCCGAACGTGTCACGT-3′. These sequences were cloned into the lentiviral vector GV493 containing sequences of hU6-MCS-CBh-gcGFP-IRES-puromycin. GH_3 cells were transduced with supernatants containing virus carrying the shMeCP2 or shhnRNP L construct using the Lipofectamine 3000 reagent (Invitrogen). After 48 h, the transduction effect was verified with fluorescent microscopy, and the infected cells were then selected with 10 mg/ml puromycin for 75 days.

For MeCP2 and hnRNP L co-expression, plasmid GV366 (CMV-MCS-HA-SV40-Neomycin) was used to clone full length of hnRNP L (NM_001134760) using XhoI and BamHI restriction enzymes. The plasmid GV657 (CMV-MCS-3flag-polyA-EF1A-zsGreen-sv40-puromycin) was used to clone full length MeCP2 (NM_022673) using BamHI and KpnI restriction enzymes. The control plasmid is CON237. All constructs generated were confirmed by sequencing. HEK293T cells were transiently transduced with plasmid constructs for the overexpression of MeCP2-Flag and hnRNP L-HA using the Lipofectamine 3000 reagent (Invitrogen).

Western blotting

Total or nuclear proteins of cell lysates were subject to SDS polyacrylamide gel electrophoresis, and blotted onto PVDF membranes (Millipore, IPVH00010). After blocking with 5% skimmed milk, the membrane was incubated overnight with the primary antibodies at 4°C, and then followed by horseradish peroxidase-conjugated secondary antibody and detected by chemoluminescence using ECL reagent (BIO-RAD, 1705061). The primary antibodies included anti-MeCP2 (CST, 3456), anti-hnRNP L (Santa Cruz, sc-32317), anti-METTL3 (Abcam, ab195352), anti-hnRNP F/H (Santa Cruz, sc-32310) and anti-GAPDH (Abcam, ab181602).

Nuclear protein extraction and co-immunoprecipitation

HEK293T cells were washed twice in ice-cold PBS and re-suspended in NP-40 buffer (75 mM NaCl, 0.325% NP-40, 1 mM EDTA, 10 mM Tris–Cl; pH 7.5) with Halt™ protease and phosphatase inhibitor cocktail (Thermo Scientific,

78441). The suspension was gently pipetted until no visible pellet, incubated on ice for 30min, and centrifuged at 2400 × g for 10 min at 4°C. The resulting pellet was washed twice with ice-cold PBS, resuspended in lysis buffer (25 mM Tris, 150 mM NaCl, 1% NP-40, 1.5 mM $MgCl_2$; pH 8.0) and sonicated with a regimen of ten 1-s pulses at 4°C, and treated with Benzonase (Merck Millipore, 70746) and DNase I (Thermo Scientific, EN0521) at room temperature for 1h.

Co-immunoprecipitation for the MeCP2-Flag and hnRNP L-HA interaction was performed using a Pierce™ Co-IP Kit (Thermo Scientific, 26149) following manufacturer's protocol. Briefly, anti-FLAG (Sigma, F1804) or anti-HA (CST, 3724) antibodies were immobilized onto the AminoLink Plus Coupling Resin. The nuclear lysate was pre-cleared with control agarose beads before the antibody-resin addition and overnight incubation at 4°C. The resin-protein complex was then washed twice in IP Wash Buffer (25 mM Tris, 150 mM NaCl, 1 mM EDTA, 1% NP-40, 5% glycerol; pH 7.4), followed by a final wash in 1 × Conditioning Buffer (pH 7.2), then incubated with 40 µl of Elution Buffer (pH 2.8) at room temperature for 5 min. The resulting elute was mixed with 10 µl of loading buffer (300 mM Tris•HCl, 5% SDS, 50% glycerol, pH 6.8) and heated at 100°C for 5 min for western blot analysis.

Genome/transcriptome analysis of the datasets from wild type or Rett syndrome mice

We analyzed the DNA methylation or alternative splicing of the hippocampal tissue samples of wild type or Rett syndrome mice using the raw reads from two published datasets (19,53). Briefly, we analyzed the raw reads of RNA-Seq sequences from the total RNA of the hippocampi of male littermate mice (wild type and *Mecp2*-null mice) at 7 weeks of age upon KA treatment by intraperitoneal injection (19), and the raw reads of WGBS from gDNA of the hippocampal dentate gyri of 8–10-week-old male mice (C57BL/6, same as the *Mecp2*-null background) (53). The reads were quality-controlled by FASTQC, trimmed and mapped to the mouse assembly GRCm38 (mm10) for DEXSeq or BSMAP analyses.

RNA samples from Rett syndrome patients

Usage of the patient samples in the study was under the approval of the Health Research Ethics Board of the University of Manitoba. Total RNA samples were isolated from human hippocampus and cerebellar tissues using TRIzole (Life Technologies), as we reported (54,55). Briefly, 0.5 ml of TRIzol was added to the frozen brain powders of about 50 mg in each tube, then homogenized and incubated for 5 min at room temperature. We then added 0.1 ml chloroform, incubated it for another 3 min, and centrifuged for 15 min (12 000×g, 4°C). We collected the aqueous phase and added 5 µg RNase-free glycogen and 0.25 ml isopropanol, incubated it for 10 min at room temperature, and centrifuged for 10 min (12 000×g, 4°C). We washed the pellet with 0.5 ml of 75% ethanol and centrifuged for 5 min, 12 000×g, 4°C. RNA pellets were air-dried and re-suspended in 30 µl of RNase-free water, quantified by NanoDrop 2000 micro-volume spectrophotometer, and stored at –80°C before RT-PCR. The Rett Syndrome human brain tissues used in this study are:

NIH#	RTT	Age (years)	Sex	PMD
*	T158M	13	F	<6 h
*	A201V	19 F 24 h		
4516	R255X 21	F	9 h	
1815	IVS3-2A > G	18	F	5 h
5723	Not available	22	F	6 h

*Donated brain tissues to the Rastegar lab for research (54,55).

Statistical tests

We used two-tailed Student's *t*-test, except for the built-in tests in DAVID (modified Fisher's exact test). The DEXSeq uses Fisher's test (42).

Data availability

The raw reads of RNA-Seq of RNA, WGBS of DNA, extracted from the rat pituitary GH_3 cells with differential treatments are available at Sequence Read Archive (SRA) database: https://www.ncbi.nlm.nih.gov/bioproject/PRJNA701032.

Results

Adaptive splicing induced by ITD of GH_3 pituitary cells and its disruption by the DNA methylation inhibitor 5-azacytidine

The depolarization effect on splicing is reversible by washing off/adding back depolarizing concentrations of KCl (50 mM) (41). We thus mimicked interval-training activities of cells by treating GH_3 pituitary cells with interval-training depolarization (ITD), in comparison to the single round of treatment established in these cells in our previous studies (11,12). The cells were treated once or six times with depolarizing concentrations of KCl for 6h, followed by 18h wash-off intervals (Figure 1A, see also S_Figure 1A and B for pre-tests of the STREX exon (10)). Our treatment did not alter the growth curve of the cells (S_Figure 1C), and showed strong homeostatic expression for the majority of exons (99%, S_Figure 1D) and the signature *Prolactin* and *Growth hormone* genes of the pituitary cells (56) (see below).

A subset of exons (1878 exons of 1204 genes) displayed substantial changes from the 1st KCl treatment (Figure 1B), in contrast to the continued exon repression upon sustained KCl treatment up to 24 h without wash-off (41) (see also S_Figure 1A). Around 81% of them were alternatively spliced exons and the remainder were produced from alternative transcription start or polyadenylation sites. These genes mainly clustered for functions at the synapse or for RNA recognition (S_Figure 1E). Their alternative exons exhibited three primary response patterns upon ITD: homeostatic, desensitized, or hypersensitive compared to their responses to the single (1st) KCl treatment (S_Figure 1F–H). Validation by semi-quantitative reverse transcription-polymerase chain reaction (RT-PCR) confirmed adaptive splicing in 78.3% of exons ($n = 23$) examined by their altered net percent changes of exon inclusion upon ITD over the 1st treatment (Supplementary Figure S1G and H, desensitized or hypersensitive, $P < 0.05$ by Δ%). Therefore, ITD induces adaptive splicing of a group of exons in genes associated with key cellular functions amidst the homeostatic response of most exons.

In subsequent tests of several pathway inhibitors including the known calcium signaling inhibitor nifedipine in

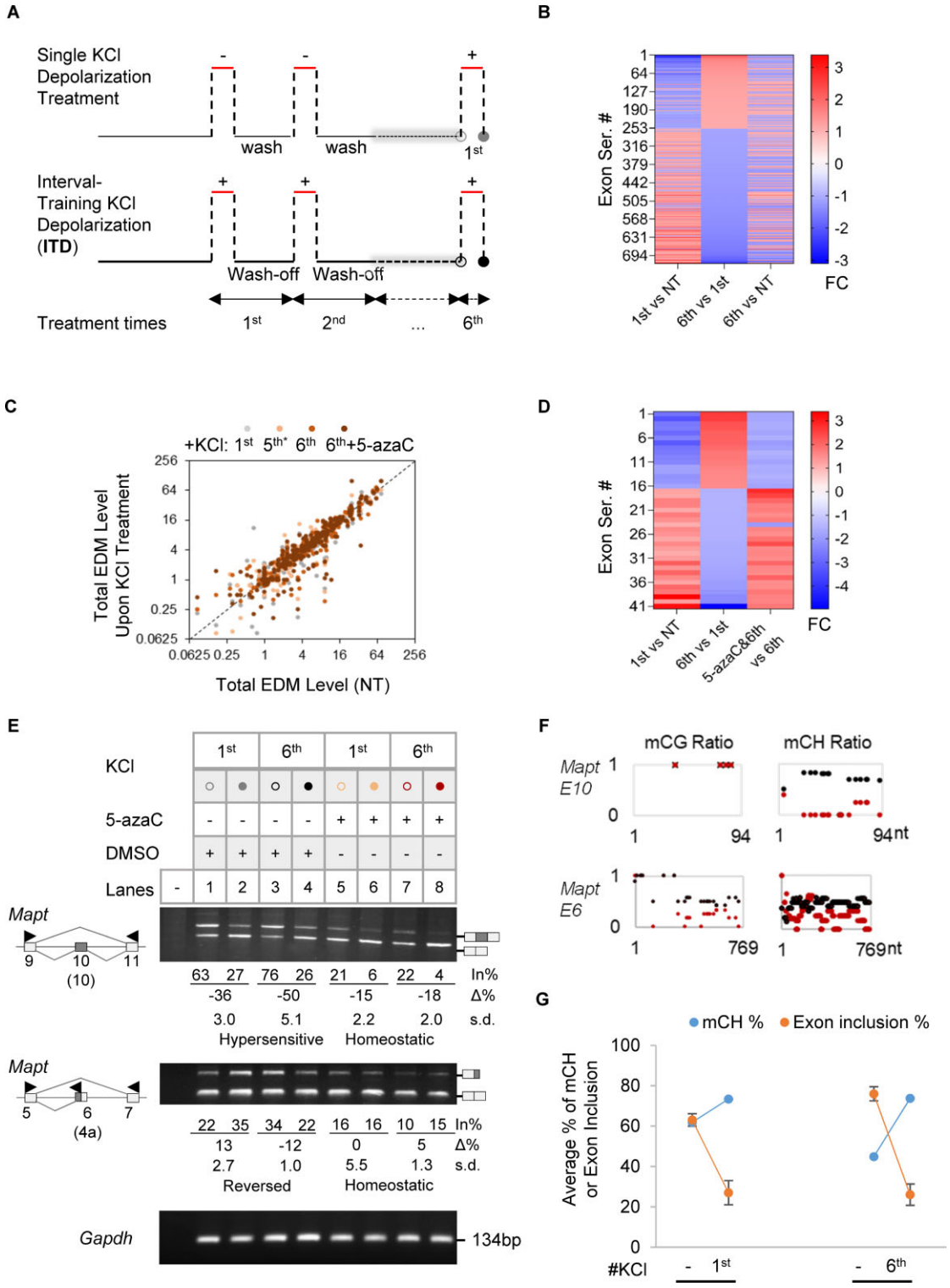

Figure 1. Adaptive splicing of a group of exons upon ITD of GH_3 pituitary cells and effect of the DNA methylation inhibitor 5-azacytidine. (**A**) Scheme of the single or ITD KCl (50mM) treatments of GH_3 pituitary cells. (**B**) Heatmap of the fold changes (FC) of 720 exons between the 6th and 1st KCl-treated cells by DEXSeq analysis (≥1.1-fold, $P < 0.01$, average base mean >20, exon base mean >20). Additional exons were detected by MATS analysis. (**C**) EDM levels upon the 1st or ITD KCl treatments versus their levels in NT samples by BSMAP analysis of WGBS data ($n = 346$ exons with measurable mC in all samples). Grey, yellow, orange or red dot: 1st, 5th, 6th and 6th KCl plus 5-azaC treatment, respectively. *: 18 h after wash-off of the 5th KCl media, before the 6th KCl addition. NT, not treated. (**D**) Heatmap of the usage fold changes of 41 top adaptive exons (FC > 1.5) that are prevented by 5-azaC (FC > 1.5). (**E**) Representative agarose gels of RT-PCR products (Left) of 5-azaC effects on the adaptive splicing of exons in response to single round of depolarization or ITD treatments ($n \geq 3$). Arrowheads: PCR primers. The exon numbers are based on reference transcripts in the UCSC Genome Rat Jul. 2014 (RGSC 6.0/rn6) Assembly: Mapt exon 6, M84156, equivalent to human MAPT exon 4a (NM_001123066.3, GRCh38/hg38); Mapt exon 10, M84156, equivalent to human MAPT exon 10 (NM_001123066.3, GRCh38/hg38). The changes by depolarization (Δ%) are all significant except for the Mapt exon 6(4a) with 5-azaC treatment. (**F**) The corresponding mC ratios of the exons in **E** upon the 6th KCl treatment with (red) or without (black) 5-azaC. (**G**) An example of EDM changes (*Mapt* exon 10, in 100% scale) by the 1st and 6th depolarization treatment, alongside its exon inclusion levels.

the depolarization-regulated splicing (13) (Supplementary Figure S2), 5-azacytidine (5-azaC), an inhibitor of DNA methyl-transferases (DNMT) (57,58), significantly disrupted splice site usage (59) and the adaptive splicing of endogenous exons (Figure 1C-F, and Supplementary Figure S3). The adaptive synaptic exons (S_Figure 1E) together with epigenetic effects in neurological diseases (37), also made the 5-azaC effect an interesting direction for further investigation.

Specifically, prior addition of 5-azaC to the cells before the 6th KCl treatment led to global alterations in exonic DNA methylation (EDM) and exon usage, which inversely correlated with each other overall (S_Figure 3A and B). Consistent with these effects, KCl depolarization itself indeed also caused EDM changes in across 346 exons detected along the course of the treatments compared to that of the non-treated (Figure 1C). Importantly, 41 of the top 52 adaptive exons (~79%) were disrupted by at least 1.5 folds when treated with 5-azaC (Figure 1D). RT-PCR analysis confirmed that the adaptive splicing of these exons was mostly abolished to homeostatic responses by 5-azaC (Figure 1E and Supplementary Figure S3C), and two of their response patterns reversed (Dlg and Phldb1 exons). More interestingly, we also noticed that even some homeostatically responsive exons became adaptive upon the 5-azaC treatment (e.g. STREX in Supplementary Figure S1G and Mapt E7a in Supplementary Figure S3C). The 5-azaC effect on the patterns of splicing responses to ITD was accompanied by EDM changes (Figure 1F, G, and S_Figure 3D). Together, these data suggest that EDM probably play a role in the ITD-induced patterns of adaptive or homeostatic splicing in an exon-specific manner.

EDM level-dependent adaptive or homeostatic splicing of *in vitro* methylated exons

To directly explore the influence of EDM on adaptive or homeostatic splicing, we created synthetic reporter exons harboring either 3 or 7 copies of CpG dinucleotides that can be specifically methylated *in vitro* (Figure 2A, from exon 14 of the synaptic m*Baiap2* gene (60)). The methylation efficiency reached at least 90% (Figure 2B) by the M. SssI CpG methyltransferase (61). The reporters with various EDM levels were tested with co-expressed CaMKIV, a key mediator of depolarization-induced splicing (10,12,13,15,41).

Upon co-transfection into HEK293T cells with the constitutively active Flag-CaMKIV-dCT or its kinase-dead mutant (12,13,17), we observed that the $(CpG)_{\times 3}$ exon was repressed by CaMKIV by approximately 20% reduction, regardless of its methylation status, consistent with a homeostatic response (Figure 2C, lanes 1–4). However, increasing the CpG count to 7, resembling the ITD-induced EDM changes (Figure 1C, F–G), augmented the CaMKIV repression from 34% to 51% reduction upon hypermethylation, consistent with a hypersensitive response (lanes 5–8). In contrast, mutating the additional 4 copies of CpG dinucleotides eliminated this enhancement effect, reversing it back to homeostatic response (lanes 9–12). This indicates that the EDM level determines the exon's homeostatic (lanes 1–4, 9–12) or adaptive (lanes 5–8) response to the same stimulation by the co-expressed CaMKIV, and the EDM change is both necessary and sufficient for an altered/adaptive splicing response to CaMKIV. Taken together with the ITD-induction of EDM changes and their correlation with the splicing changes (Figure 1C, G and S_Figure 3A–B, D), these results support an essential role of EDM level and its changes in ITD/CaMKIV-induced adaptive or homeostatic splicing.

Essential role of MeCP2 and its partner hnRNP L in ITD-induced adaptive or homeostatic splicing of a group of exons

Based on the EDM analysis, the roles of the mC-binding MeCP2 and CaMKIV-target splicing factor hnRNP L in activity-dependent splicing (10,19), and synaptic gene exons changed by both 5-azaC and hnRNP L (40) (Supplementary Table S1), it's likely that MeCP2 and hnRNP L are involved in the ITD-induced splicing patterns as well. Interestingly, these two proteins interact in reciprocal co-immunoprecipitation assays (Figure 3A). We thus established GH_3 cell colonies stably knocked down of MeCP2 or hnRNP L using lentiviral shRNAs (Figure 3B and C). Upon knockdown of either factor, all five adaptive exons of the synaptic genes tested lost their adaptive splicing patterns to homeostatic responses to ITD (Figure 3D-E), in a similar way as the same *Epb41l3*, *Nrg1* and *Mapt* exons by 5-azaC in Supplementary Figure S3C and Figure 1E. The homeostatic STREX exon (see also Supplementary Figure S1G), in contrast exhibited desensitized or hypersensitive responses to ITD upon knockdown of the two factors, respectively.

In further support of hnRNP L's role in the control of additional adaptive/homeostatic exons besides the reported STREX (10,17,40), we examined the sequences of the 119 exons regulated by both hnRNP L and 5-azaC (Figure 4A and Supplementary Table S1). They share specifically an hnRNP L-preferred CA-rich consensus motif in or nearby the exons (Figure 4B). Moreover, UV-crosslinking-immunoprecipitation and CA-to-CG mutation assays of the *Mapt* exon 6 motif at the 3′ splice site supported hnRNP L direct binding to the site in a CA-dependent manner (Figure 4C). In the WGBS analysis (Figure 1C), the mC ratio around the 3′ splice site of the Mapt exon 6 (4a) changed from 0.75 to 0.54 by the 1st and 0.66 to 1.0 by the 6th KCl treatment, respectively, and then reduced to 0.29 by 5-azaC.

Together, these findings support that both MeCP2 and its associated hnRNP L are required for either adaptive or homeostatic splicing responses of the synaptic alternative exons upon ITD.

Essential role of MeCP2 for the homeostatic splicing and expression of the *Prolactin* hormone gene upon ITD of the pituitary cells or for the proper splicing of the adaptive exons of synaptic genes in the hippocampus of Rett syndrome patients

In addition to disrupting ITD-dependent adaptive or homeostatic splicing, we also found that treatment with 5-azaC exacerbated aberrant splicing of a number of hormone or hormone-related genes including the *Prolactin* gene upon ITD, accompanied by EDM changes (Supplementary Figures S4–S6). This observation suggests disruption of the homeostatic splicing of even the constitutive exons during ITD upon epigenetic changes. We thus examined the *Prl* transcripts in the MeCP2-knockdown cells and found significantly increased *Prl* transcript level and exacerbated aberrant splicing, both in an ITD-dependent way (Figure 5A). Particularly

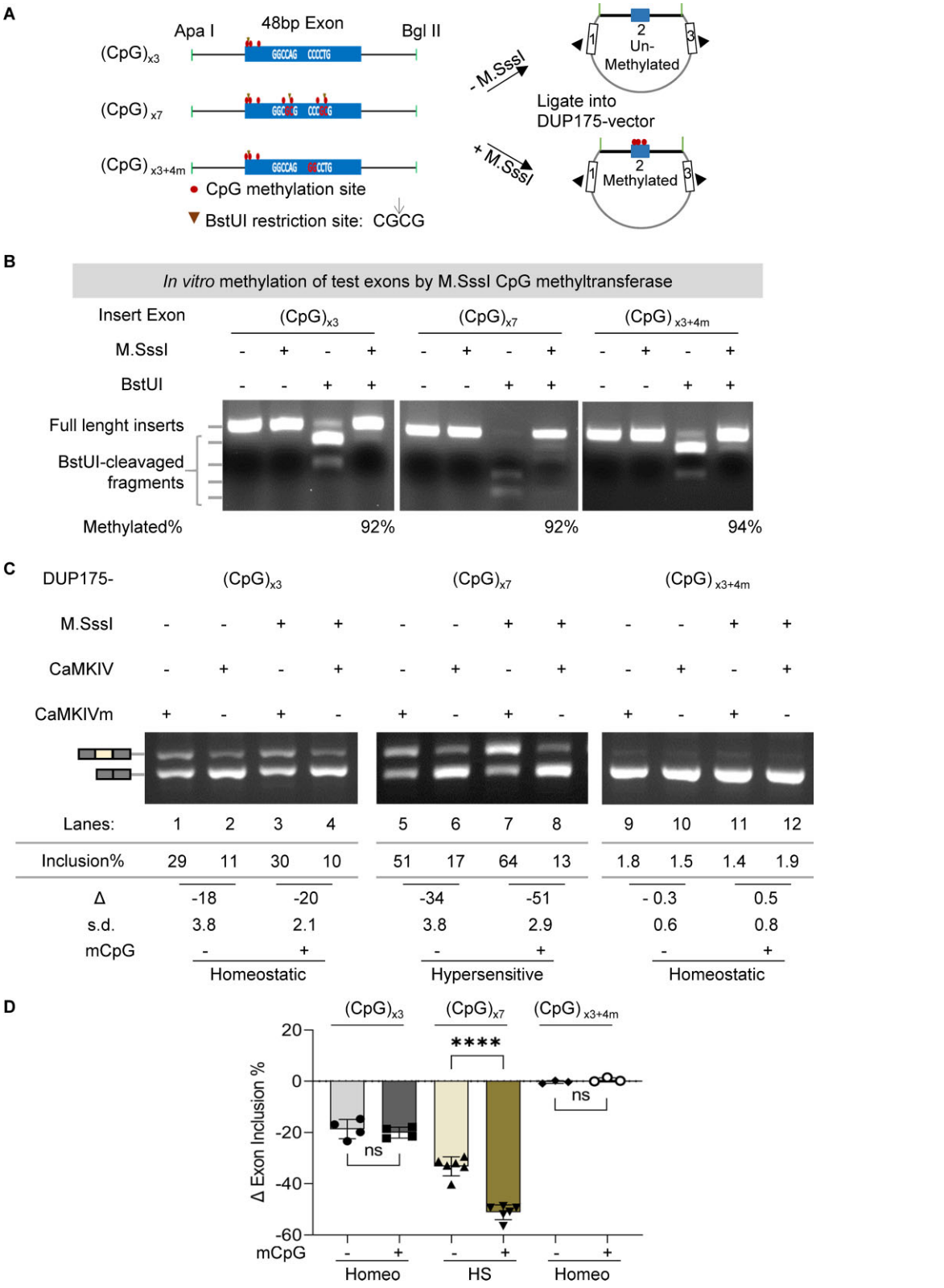

Figure 2. Effect of the EDM status on the adaptive or homeostatic splicing in response to CaMKIV. (**A**) Diagram of the *in vitro* EDM minigene splicing reporter assay. The synthesized reporter exons are based on the adaptive exon 14 (48nt, ENSMUST00000106233.1, GRCm38/mm10) of the mouse *Baiap2* gene (see below). Its partial flanking introns here do not harbor CpG sites. The vector backbone is the DUP175, derived from the constitutive beta-globin exons. Arrowheads: PCR primers. (**B**) The *in vitro* methylation efficiency of the reporter exons [$(CpG)_{x3}$, $(CpG)_{x7}$ or $(CpG)_{x3+4m}$] by M. SssI CpG methyltransferase, verified by using the CpG methylation-sensitive BstUI (restriction site: CG↓CG). The percentage of the full-length insert (minus the uncleaved full-length, unmethylated insert in the preceding lane) out of all fragments in each lane was taken as the methylation efficiency. (**C**) Agarose gels of semi-quantitative RT-PCR products of the splicing reporters transiently expressed in HEK293T cells with CaMKIV or its mutant (CaMKIVm). (**D**) Bar graph of net percent changes of the reporter exons in (C) by CaMKIV ($n \geq 3$). Homeo: homeostatic; HS: hypersensitive; ns: not significant; ****$P < 0.0001$.

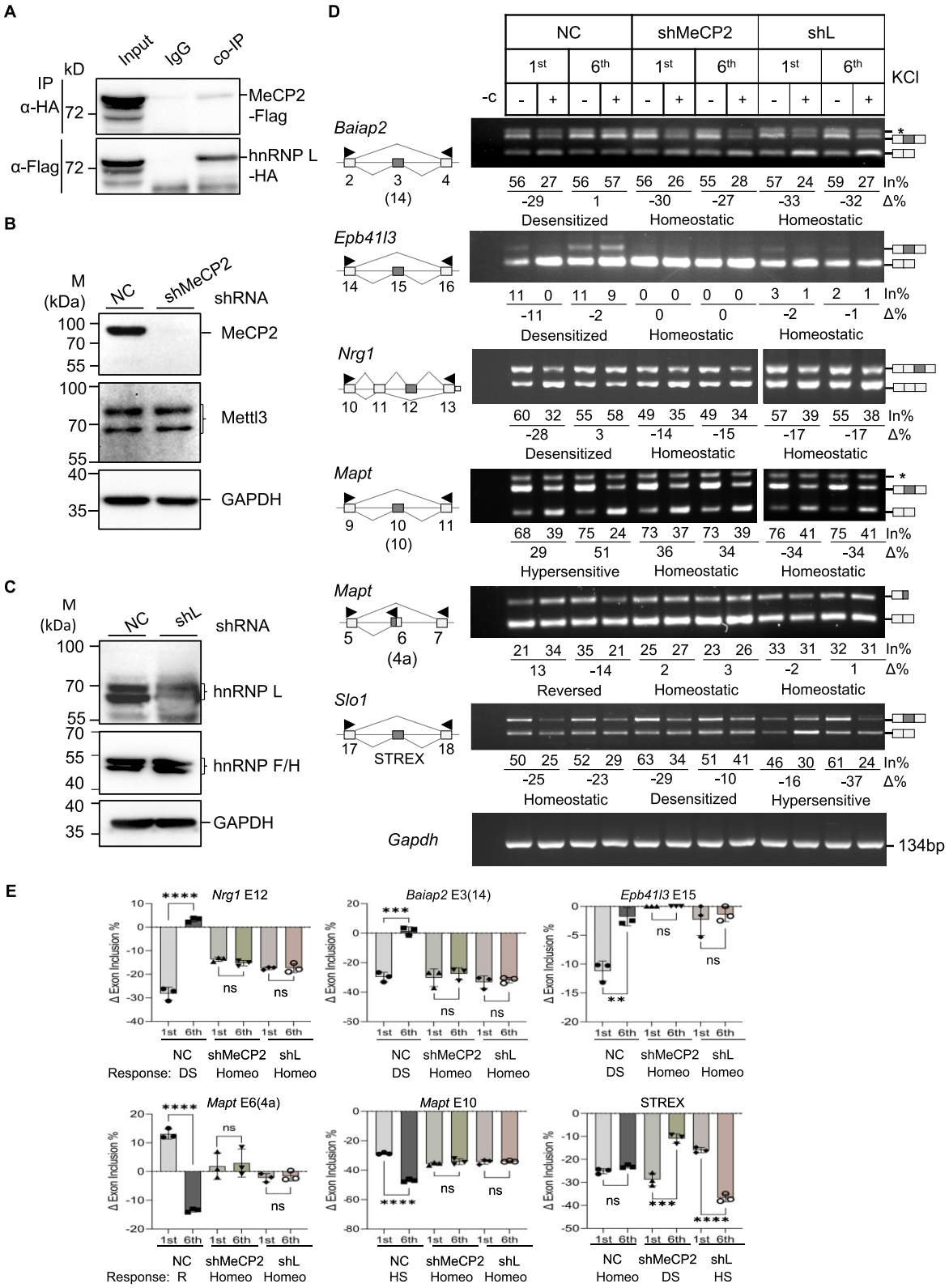

Figure 3. Effect of knocking down MeCP2 or its partner hnRNP L on adaptive or homeostatic splicing. (**A**) Reciprocal co-immunoprecipitation assay of MeCP2-Flag and hnRNP L-HA co-expressed in HEK293T cells. IgG: rabbit IgG, negative control. (**B, C**) Western blot analyses of stable lentiviral shRNA-expressing GH_3 cell lines showing specific knockdown of MeCP2 (B) or hnRNP L (C) proteins compared to the non-targeting control shRNA (NC). Mettl3, hnRNP F/H and GAPDH are shRNA-negative and protein loading controls. (**D**) Representative agarose gels of RT-PCR products of the major patterns of MeCP2 or hnRNP L knockdown effects on the adaptive or homeostatic response of exons that are also disrupted by 5-azaC ($n \geq 3$) in GH_3 cells. Arrowheads: PCR primers. (**E**) Bar graphs of net percent changes of adaptive or homeostatic exons upon single (1^{st}) or ITD (6^{th}) KCl treatment, with/without MeCP2 or hnRNP L knockdown ($n \geq 3$). Homeo: homeostatic; DS: desensitized; HS: hypersensitized; R: reversed. ns: not significant, $^{**}P < 0.01$; $^{***}P < 0.001$; $^{****}P < 0.0001$.

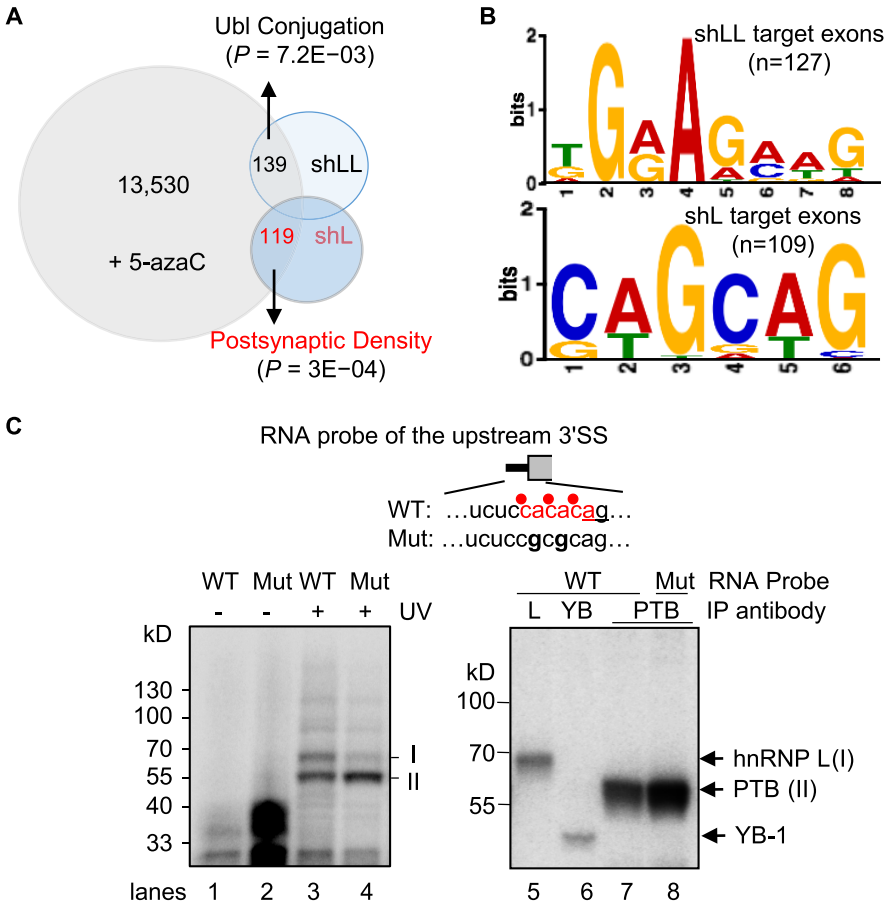

Figure 4. hnNRP L-binding motifs of exons changed in 5-azaC-treated and in hnRNP L-knockdown GH_3 cells. (**A**) Diagram of differentially spliced exons in the GH_3 transcriptome upon 5-azaC treatment of the 6th KCl samples (Figure 1C) or upon lentiviral knockdown of hnRNP L protein by shL, with the L-like (LL) targets in comparison. (**B**) Consensus motifs of shLL- or shL-changed exons that were also affected by 5-azaC, identified by MEME analysis. (**C**) UV crosslinking of wild type (WT) CA repeat or CG mutant (Mut) RNA probes of the *Mapt* exon E6 upstream 3′ splice site in HeLa nuclear extracts. Upper: probe diagram. Red dots: corresponding DNA mCpAs, of which methylation levels were reduced by 5-azaC. Underlined: 3′ AG. Lower: phosphorimages of proteins crosslinked to the probes and resolved in SDS-PAGE gels. Immunoprecipitating antibody is against hnRNP L (L), YB-1 (YB) or PTB (PTBP1). A sixth of the crosslinking mix for immunoprecipitation was loaded in lanes 3 and 4.

the aberrant splicing includes the skipping of constitutive exons 2 and 3 coding for the conserved domain of the growth hormone-like superfamily (40,62), or the inclusion of a cryptic 93nt exon also found in hnRNP L-knockdown cells (40). In contrast, the growth hormone *Gh1* gene expression and splicing were not affected in these cells. Thus, the homeostatic splicing and expression of the pituitary cell's signature gene *Prolactin* specifically requires sufficient MeCP2 in response to ITD. This finding of the ITD-aggravated effect not only aligns closely with but also goes beyond the *MECP2* mutation-aggravated aberrant splicing induced by chronic neuronal activities with sustained treatment (19), as well as with abnormal neuronal activities and synaptic plasticity associated with the progression of Rett syndrome (31,63–66). Moreover, the increased *Prl* mRNA transcripts upon MeCP2 knockdown may help explain the origin of the hyperprolactinemia in about 14% of the Rett syndrome patients (67,68). Together our findings support that MeCP2 is critical for the maintenance of homeostatic splicing and steady expression of the prolactin hormone transcript upon ITD in the pituitary cells.

To corroborate these *in vitro* findings from cultured cells, we evaluated the splicing of the ITD-induced adaptive exons in MeCP2-defective mouse or human samples. In *Mecp2*-null mice (19,53), the calcium signal-activator kainic acid (KA) generally exacerbated splicing changes (Supplementary Figure S7A), consistent with previous studies (19). Interestingly, these splicing alterations were also inversely correlated with EDM globally, including 8 of the top adaptive exons affected by 5-azaC (from Figure 1D). Importantly, we identified several of the adaptive exons in Rett syndrome patients with *MECP2* mutations (29,64,69). These exons, particularly the synaptic *EPB41L3* exon 15, showed significant splicing changes in the hippocampi but not cerebella of patients (Figure 5B, and Supplementary Figure S7B–D), although with differences from the pituitary cells (Figures 1 and 3C, and Supplementary Figure S3), a context-dependent effect (70). Nonetheless, this result indicates that at least a group of the ITD-induced adaptive exons also undergo hippocampus-specific aberrant splicing upon loss-of *MECP2* function.

Taken together, the epigenetic control is likely essential for both adaptive and homeostatic splicing of alternative exons and the homeostatic splicing and expression of the signature *Prolactin* hormone gene upon ITD of pituitary cells, with implications for the aberrant splicing of such exons in the progressive genetic disease Rett syndrome.

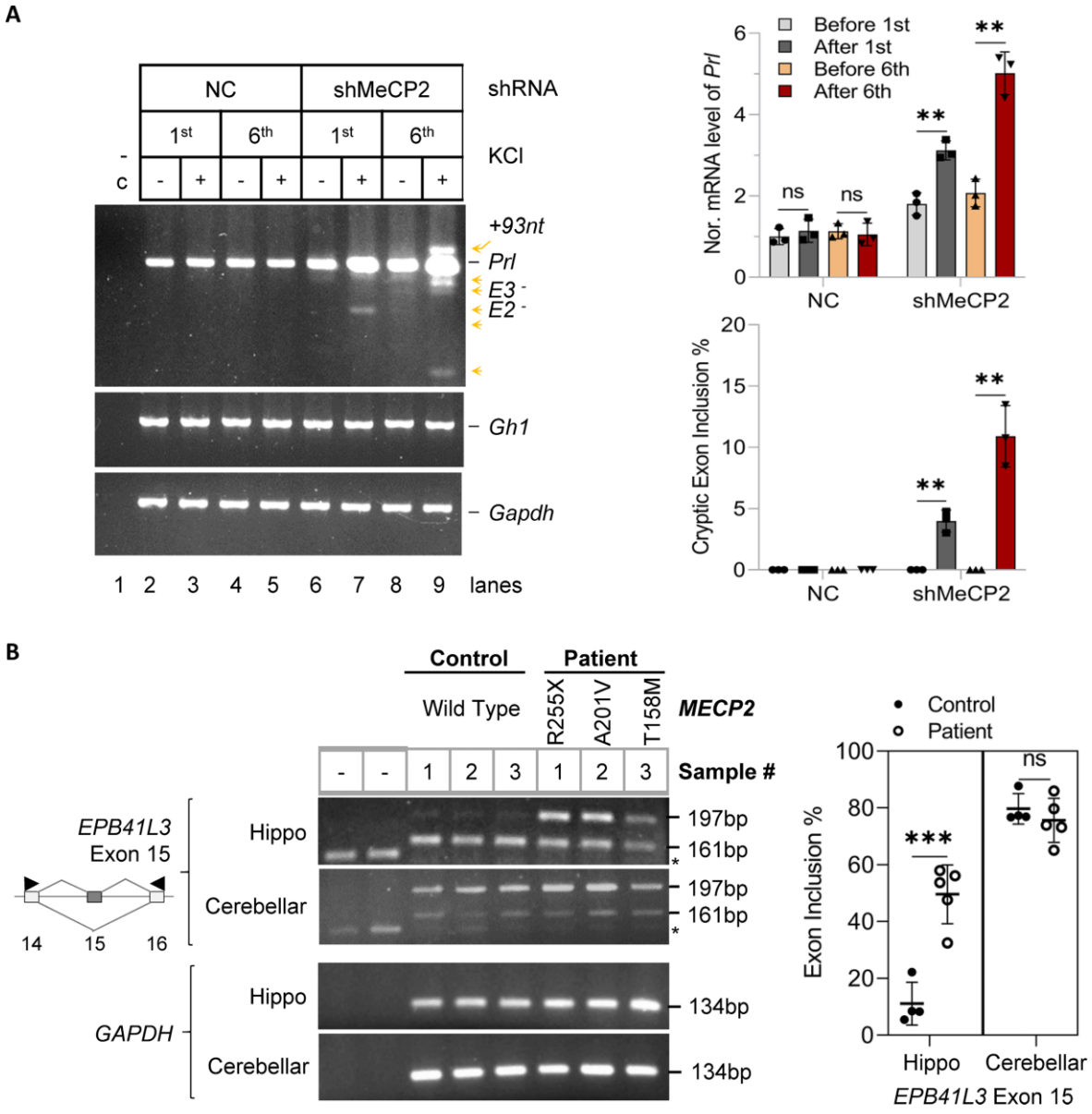

Figure 5. Exacerbated overexpression and aberrant splicing of the *Prolactin* gene in MeCP2-knockdown GH_3 cells upon ITD and aberrant splicing of the adaptive exons of synaptic genes in Rett syndrome patients. (**A**) RT-PCR products of the hormone *Prolactin* (*Prl*) gene upon MeCP2 knockdown and ITD treatment of GH_3 pituitary cells. *Gh*: growth hormone gene as a negative control of the hormone genes; *Gapdh*: RNA loading control. Arrowheads: aberrant splice variants with the deduced cryptic skipped/included exons to the right. +93nt: inclusion of a 93nt cryptic exon in the *Prl* intron 4 as reported by Lei, et al., *MCB*'18. RNA samples are as in Figure 3B and D. The bar graph to the right shows the ITD-dependent increase of not only the level of the *Prolactin* mRNA transcript normalized to *Gapdh* (Top), but also its aberrant transcripts with exons skipped or the intron fragment included (Bottom). (**B**) (Left) Agarose gel RT-PCR products of the adaptive *EPB41L3* synaptic gene/exon in the hippocampal tissues (Hippo) of Rett syndrome patients and healthy controls. Cerebella of the same individuals are tissue controls. *: Product from primers without cDNA input. (Right) Bar graphs of the percentages of exon inclusion (mean ± s.d., $n = 5$ Rett syndrome patients, and 4 healthy controls). ns: not significant; $^{**}P < 0.01$; $^{***}P < 0.001$.

Discussion

Traditionally, studies on gene expression and particularly alternative splicing have focused on the effects of single or continuous treatments. However, cells often experience repeated extracellular stimuli interrupted by periods of inactivity, as seen in neurons, muscle cells and hormone-producing pituitary cells in such activities as interval-training exercises or drug addiction (1,2,5). Our study extends the existing body of work by examining how cells adapt their alternative splicing pattern in response to interval-training depolarization (ITD) while maintaining their identity by homeostatic gene expression and splicing responses. The ITD perhaps did not recapitulate the physiological stimuli precisely in terms of strength and duration but it does provide a proof-of-principle for interval training activity-dependent splicing regulation that is different from the sustained treatment on exons (19,41). The results here demonstrate clearly that exons may exhibit different responses to cell activities depending on how many times the cells are stimulated, likely due to altered epigenetic and splicing components (Figures 1C, 3 and 5A). The altered patterns of splicing responses would likely allow cells to fine-tune their adaption during such activities as exercises

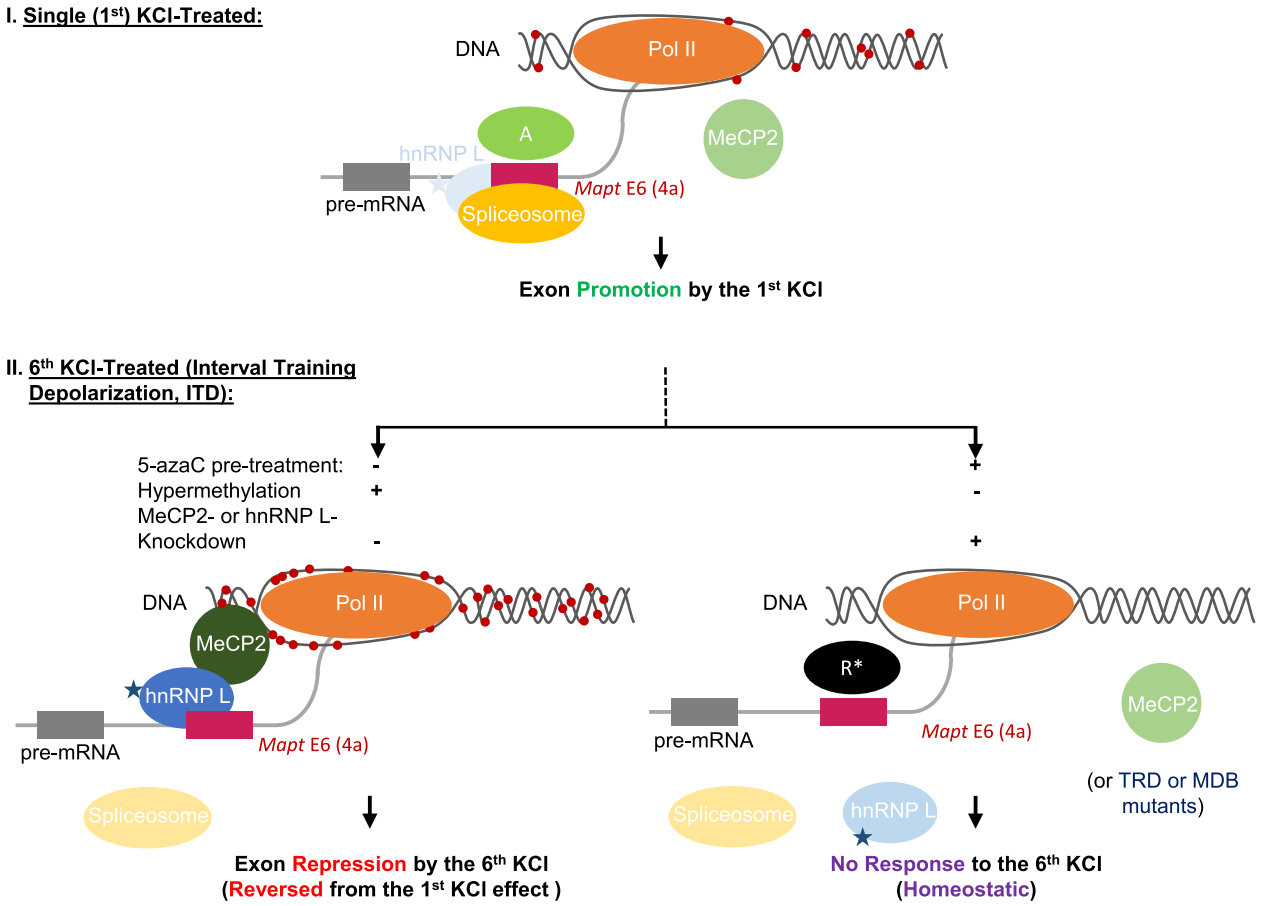

Figure 6. Summary of the epigenetic components in the control of adaptive or homeostatic splicing upon ITD. Shown are effects on the *Mapt* exon 6 (4a) as an example of the exon-dependent, diverse changes of methylation/splicing. With a single round of KCl treatment (I), the DNA methylation at the 3′ splice site is at a comparatively low level (54%); therefore, binding of MeCP2 and its associated hnRNP L to the DNA and pre-mRNA is inefficient, and insufficient to overcome the effect of splicing activators (**A**) in cells. Upon the 6th KCl-treatment (II, ITD), the DNA is hypermethylated (100%, Left panel) recruiting MeCP2 and its associated hnRNP L leading to exon repression (reversed splicing response from the 1st KCl treatment). Right panel: with 5-azaC pre-treatment (Figure 1E, F), the methylation is greatly reduced (29%) and the exon is inhibited by a depolarization non-responsive repressor (R) thereby homeostatic splicing response. *: In case of MeCP2- or hnRNP L-knockdown (Figure 3D), the repressor R is likely replaced by a depolarization-non-responsive activator also causing homeostatic splicing though with higher basal level of the exon. Similar decoupling of the methyl-DNA/MeCP2 and associated hnRNP L is likely most effective when the TRD and MDB domains of *MECP2* are mutated (Supplementary Figure S7D). The mC changes and their disruption during the adaptive splicing are also consistent with the *in vitro* methylation/mutagenesis data of the reporter exon in Figure 2. Star: p-Ser^{513} of hnRNP L by CaMKIV. Red dots on DNA: methyl-Cytosines. Lighter colors of the factors/spliceosomes represent their reduced effects.

or stress in endocrine cells (2,3,5,6), and to electrical firing activities in neurons (11,12,14–16). The dysregulation of the adaptive/homeostatic splicing upon epigenetic disruption (Figure 5) likely contribute to the aberrant gene expression or splicing in the progression of neurological diseases. The diverse effects of the epigenetic control of different exons probably suggest an important role of the exon-dependent interplay between the epigenetic and splicing machineries (Figure 6) in adaptive and homeostatic cell physiology and progressive diseases. The interplay is worthy of further study for the exon-dependent effect and underlying molecular mechanisms that may involve more epigenetic/splicing factors in the process (Supplementary Figure S8 and Supplementary Tables S2 and S3).

Data availability

The raw reads of RNA-Seq of RNA, WGBS of DNA, extracted from the rat pituitary GH3 cells with differential treatments are available at Sequence Read Archive (SRA) database: https://www.ncbi.nlm.nih.gov/bioproject/PRJNA701032.

Supplementary data

Supplementary Data are available at NAR Online.

Acknowledgements

We thank the University of Maryland Brain and Tissue Bank, a Brain and Tissue Repository of the NIH Biobank (at NIH NeuroBioBank Program: neurobiobank.nih.gov), and the patient families who donated brain tissues for research, and Frederick Robidoux and Sylvie Laboissiere of the McGill University Genome Quebec Innovation Centre for their excellent service. We thank Dr. Chunyu Liu for helpful comments on the manuscript. The work has been supported by a Manitoba Research Chair fund, a CIHR (Canadian Institutes of Health Research) operating grant FRN_106608, and in part

by NSERC (Natural Sciences & Engineering Research Council of Canada) discovery grants (RGPIN-2016-06004 and -2022-05023) to J.X., and by University of Manitoba Rady Innovation Funds to M.R. and J.X., and NSERC-DG grant (2016-06035) to M.R. L.L., U.D. and S.O. by UMGF scholarships, and S.O. by a Vanier Graduate Scholarship.

Funding

CIHR (Canadian Institutes of Health Research) operating grant [FRN_106608]; University of Manitoba Rady Innovation Funds; NSERC (Natural Sciences & Engineering Research Council of Canada) discovery grants [RGPIN-2016-06004, RGPIN-2022-05023]; Manitoba Research Chair fund; NSERC-DG [2016-06035]. Funding for open access charge: NSERC.

Conflict of interest statement

None declared.

References

1. Browne,C.J., Godino,A., Salery,M. and Nestler,E.J. (2020) Epigenetic mechanisms of opioid addiction. *Biol. Psychiatry*, **87**, 22–33.
2. Wideman,L., Weltman,J.Y., Hartman,M.L., Veldhuis,J.D. and Weltman,A. (2002) Growth hormone release during acute and chronic aerobic and resistance exercise: recent findings. *Sports Med.*, **32**, 987–1004.
3. MacInnis,M.J. and Gibala,M.J. (2017) Physiological adaptations to interval training and the role of exercise intensity. *J. Physiol.*, **595**, 2915–2930.
4. Moore,T.M., Lee,S., Olsen,T., Morselli,M., Strumwasser,A.R., Lin,A.J., Zhou,Z., Abrishami,A., Garcia,S.M., Bribiesca,J., *et al.* (2023) Conserved multi-tissue transcriptomic adaptations to exercise training in humans and mice. *Cell Rep.*, **42**, 112499.
5. Egan,B. and Zierath,J.R. (2013) Exercise metabolism and the molecular regulation of skeletal muscle adaptation. *Cell Metab.*, **17**, 162–184.
6. Ling,C. and Ronn,T. (2014) Epigenetic adaptation to regular exercise in humans. *Drug. Discov. Today*, **19**, 1015–1018.
7. Lee,Y. and Rio,D.C. (2015) Mechanisms and regulation of alternative pre-mRNA splicing. *Annu. Rev. Biochem.*, **84**, 291–323.
8. Maniatis,T. and Tasic,B. (2002) Alternative pre-mRNA splicing and proteome expansion in metazoans. *Nature*, **418**, 236–243.
9. Blencowe,B.J. (2006) Alternative splicing: new insights from global analyses. *Cell*, **126**, 37–47.
10. Liu,G., Razanau,A., Hai,Y., Yu,J., Sohail,M., Lobo,V.G., Chu,J., Kung,S.K. and Xie,J. (2012) A conserved serine of heterogeneous nuclear ribonucleoprotein L (hnRNP L) mediates depolarization-regulated alternative splicing of potassium channels. *J. Biol. Chem.*, **287**, 22709–22716.
11. Razanau,A. and Xie,J. (2013) Emerging mechanisms and consequences of calcium regulation of alternative splicing in neurons and endocrine cells. *Cell. Mol. Life Sci.*, **70**, 4527–4536.
12. Xie,J. and Black,D.L. (2001) A CaMK IV responsive RNA element mediates depolarization-induced alternative splicing of ion channels. *Nature*, **410**, 936–939.
13. Xie,J., Jan,C., Stoilov,P., Park,J. and Black,D.L. (2005) A consensus CaMK IV-responsive RNA sequence mediates regulation of alternative exons in neurons. *RNA*, **11**, 1825–1834.
14. Li,B., Suutari,B.S., Sun,S.D., Luo,Z., Wei,C., Chenouard,N., Mandelberg,N.J., Zhang,G., Wamsley,B., Tian,G., *et al.* (2020) Neuronal inactivity co-opts LTP machinery to drive potassium channel splicing and homeostatic spike widening. *Cell*, **181**, 1547–1565.
15. Iijima,T., Wu,K., Witte,H., Hanno-Iijima,Y., Glatter,T., Richard,S. and Scheiffele,P. (2011) SAM68 regulates neuronal activity-dependent alternative splicing of neurexin-1. *Cell*, **147**, 1601–1614.
16. Penn,A.C., Balik,A., Wozny,C., Cais,O. and Greger,I.H. (2012) Activity-mediated AMPA receptor remodeling, driven by alternative splicing in the ligand-binding domain. *Neuron*, **76**, 503–510.
17. Yu,J., Hai,Y., Liu,G., Fang,T., Kung,S.K. and Xie,J. (2009) The heterogeneous nuclear ribonucleoprotein L is an essential component in the Ca2+/calmodulin-dependent protein kinase IV-regulated alternative splicing through cytidine-adenosine repeats. *J. Biol. Chem.*, **284**, 1505–1513.
18. Schor,I.E., Rascovan,N., Pelisch,F., Allo,M. and Kornblihtt,A.R. (2009) Neuronal cell depolarization induces intragenic chromatin modifications affecting NCAM alternative splicing. *Proc. Natl. Acad. Sci. U.S.A.*, **106**, 4325–4330.
19. Osenberg,S., Karten,A., Sun,J., Li,J., Charkowick,S., Felice,C.A., Kritzer,M., Nguyen,M.V.C., Yu,P. and Ballas,N. (2018) Activity-dependent aberrations in gene expression and alternative splicing in a mouse model of Rett syndrome. *Proc. Natl. Acad. Sci. U.S.A.*, **115**, E5363–E5372.
20. Sharma,A. and Lou,H. (2011) Depolarization-mediated regulation of alternative splicing. *Front. Neurosci.*, **5**, 141.
21. Halder,R., Hennion,M., Vidal,R.O., Shomroni,O., Rahman,R.U., Rajput,A., Centeno,T.P., van Bebber,F., Capece,V., Garcia Vizcaino,J.C., *et al.* (2016) DNA methylation changes in plasticity genes accompany the formation and maintenance of memory. *Nat. Neurosci.*, **19**, 102–110.
22. Nanan,K.K., Ocheltree,C., Sturgill,D., Mandler,M.D., Prigge,M., Varma,G. and Oberdoerffer,S. (2017) Independence between pre-mRNA splicing and DNA methylation in an isogenic minigene resource. *Nucleic Acids Res.*, **45**, 12780–12797.
23. Lopez Soto,E.J. and Lipscombe,D. (2020) Cell-specific exon methylation and CTCF binding in neurons regulate calcium ion channel splicing and function. *eLife*, **9**, e54879.
24. Maunakea,A.K., Chepelev,I., Cui,K. and Zhao,K. (2013) Intragenic DNA methylation modulates alternative splicing by recruiting MeCP2 to promote exon recognition. *Cell Res.*, **23**, 1256–1269.
25. Young,J.I., Hong,E.P., Castle,J.C., Crespo-Barreto,J., Bowman,A.B., Rose,M.F., Kang,D., Richman,R., Johnson,J.M., Berget,S., *et al.* (2005) Regulation of RNA splicing by the methylation-dependent transcriptional repressor methyl-CpG binding protein 2. *Proc. Natl. Acad. Sci. U.S.A.*, **102**, 17551–17558.
26. Lagger,S., Connelly,J.C., Schweikert,G., Webb,S., Selfridge,J., Ramsahoye,B.H., Yu,M., He,C., Sanguinetti,G., Sowers,L.C., *et al.* (2017) MeCP2 recognizes cytosine methylated tri-nucleotide and di-nucleotide sequences to tune transcription in the mammalian brain. *PLoS Genet.*, **13**, e1006793.
27. Kinde,B., Wu,D.Y., Greenberg,M.E. and Gabel,H.W. (2016) DNA methylation in the gene body influences MeCP2-mediated gene repression. *Proc. Natl. Acad. Sci. U.S.A.*, **113**, 15114–15119.
28. Percy,A.K., Lane,J.B., Childers,J., Skinner,S., Annese,F., Barrish,J., Caeg,E., Glaze,D.G. and MacLeod,P. (2007) Rett syndrome: North American database. *J. Child Neurol.*, **22**, 1338–1341.
29. Amir,R.E., Van den Veyver,I.B., Wan,M., Tran,C.Q., Francke,U. and Zoghbi,H.Y. (1999) Rett syndrome is caused by mutations in X-linked MECP2, encoding methyl-CpG-binding protein 2. *Nat. Genet.*, **23**, 185–188.
30. Rodriguez,L.M., Percy,A.K. and Cutter,G.R. (2020) Rett syndrome: Novel correlations linking>96% genotype, disease severity, and seizures. *Transl. Sci. Rare Dis.*, **5**, 131–141.
31. Operto,F.F., Mazza,R., Pastorino,G.M.G., Verrotti,A. and Coppola,G. (2019) Epilepsy and genetic in Rett syndrome: a review. *Brain Behav.*, **9**, e01250.
32. Gabel,H.W., Kinde,B., Stroud,H., Gilbert,C.S., Harmin,D.A., Kastan,N.R., Hemberg,M., Ebert,D.H. and Greenberg,M.E. (2015)

Disruption of DNA-methylation-dependent long gene repression in Rett syndrome. *Nature*, **522**, 89–93.
33. Juang,Y.T., Wang,Y., Solomou,E.E., Li,Y., Mawrin,C., Tenbrock,K., Kyttaris,V.C. and Tsokos,G.C. (2005) Systemic lupus erythematosus serum IgG increases CREM binding to the IL-2 promoter and suppresses IL-2 production through CaMKIV. *J. Clin. Invest.*, **115**, 996–1005.
34. Hedrich,C.M., Crispin,J.C., Rauen,T., Ioannidis,C., Apostolidis,S.A., Lo,M.S., Kyttaris,V.C. and Tsokos,G.C. (2012) cAMP response element modulator alpha controls IL2 and IL17A expression during CD4 lineage commitment and subset distribution in lupus. *Proc. Natl. Acad. Sci. U.S.A.*, **109**, 16606–16611.
35. Buchthal,B., Lau,D., Weiss,U., Weislogel,J.M. and Bading,H. (2012) Nuclear calcium signaling controls methyl-CpG-binding protein 2 (MeCP2) phosphorylation on serine 421 following synaptic activity. *J. Biol. Chem.*, **287**, 30967–30974.
36. Cheng,T.L., Chen,J., Wan,H., Tang,B., Tian,W., Liao,L. and Qiu,Z. (2017) Regulation of mRNA splicing by MeCP2 via epigenetic modifications in the brain. *Sci. Rep.*, **7**, 42790.
37. Jakovcevski,M. and Akbarian,S. (2012) Epigenetic mechanisms in neurological disease. *Nat. Med.*, **18**, 1194–1204.
38. Chhatbar,K., Cholewa-Waclaw,J., Shah,R., Bird,A. and Sanguinetti,G. (2020) Quantitative analysis questions the role of MeCP2 as a global regulator of alternative splicing. *PLoS Genet.*, **16**, e1009087.
39. Tashjian,A.H. Jr, Bancroft,F.C. and Levine,L. (1970) Production of both prolactin and growth hormone by clonal strains of rat pituitary tumor cells. Differential effects of hydrocortisone and tissue extracts. *J. Cell Biol.*, **47**, 61–70.
40. Lei,L., Cao,W., Liu,L., Das,U., Wu,Y., Liu,G., Sohail,M., Chen,Y. and Xie,J. (2018) Multilevel differential control of hormone gene expression programs by hnRNP L and LL in pituitary cells. *Mol. Cell. Biol.*, **38**, e00651-17.
41. Lee,J.A., Xing,Y., Nguyen,D., Xie,J., Lee,C.J. and Black,D.L. (2007) Depolarization and CaM kinase IV modulate NMDA receptor splicing through two essential RNA elements. *PLoS Biol.*, **5**, e40.
42. Anders,S., Reyes,A. and Huber,W. (2012) Detecting differential usage of exons from RNA-seq data. *Genome Res.*, **22**, 2008–2017.
43. Shen,S., Park,J.W., Huang,J., Dittmar,K.A., Lu,Z.X., Zhou,Q., Carstens,R.P. and Xing,Y. (2012) MATS: A Bayesian framework for flexible detection of differential alternative splicing from RNA-Seq data. *Nucleic Acids Res.*, **40**, e61.
44. Robinson,M.D., McCarthy,D.J. and Smyth,G.K. (2010) edgeR: a Bioconductor package for differential expression analysis of digital gene expression data. *Bioinformatics*, **26**, 139–140.
45. Andrews,S. (2010) In: *Babraham Bioinformatics*. Babraham Institute, Cambridge, UK.
46. Liu,L., Feng,J., Polimeni,J., Zhang,M., Nguyen,H., Das,U., Zhang,X., Singh,H., Yao,X.-J. and Leygue,E. (2021) Characterization of cell free plasma methyl-dna from xenografted tumors to guide the selection of diagnostic markers for early-stage cancers. *Front. Oncol.*, **11**, 615821.
47. Sherman,B.T., Hao,M., Qiu,J., Jiao,X., Baseler,M.W., Lane,H.C., Imamichi,T. and Chang,W. (2022) DAVID: A web server for functional enrichment analysis and functional annotation of gene lists (2021 update). *Nucleic Acids Res.*, **50**, W216–W221.
48. Bailey,T.L., Johnson,J., Grant,C.E. and Noble,W.S. (2015) The MEME suite. *Nucleic Acids Res.*, **43**, W39–W49.
49. Bailey,T.L. and Elkan,C. (1994) Fitting a mixture model by expectation maximization to discover motifs in bipolymers. *Proc. Int. Conf. Intell. Syst. Mol. Biol.*, **2**, 28–36.
50. Kammoun,F., de Roux,N., Boespflug-Tanguy,O., Vallee,L., Seng,R., Tardieu,M. and Landrieu,P. (2004) Screening of MECP2 coding sequence in patients with phenotypes of decreasing likelihood for Rett syndrome: A cohort of 171 cases. *J. Med. Genet.*, **41**, e85.
51. Chatila,T., Anderson,K.A., Ho,N. and Means,A.R. (1996) A unique phosphorylation-dependent mechanism for the activation of Ca2+/calmodulin-dependent protein kinase type IV/GR. *J. Biol. Chem.*, **271**, 21542–21548.
52. Miranti,C.K., Ginty,D.D., Huang,G., Chatila,T. and Greenberg,M.E. (1995) Calcium activates serum response factor-dependent transcription by a Ras- and Elk-1-independent mechanism that involves a Ca2+/calmodulin-dependent kinase. *Mol. Cell. Biol.*, **15**, 3672–3684.
53. Guo,J.U., Su,Y., Shin,J.H., Shin,J., Li,H., Xie,B., Zhong,C., Hu,S., Le,T., Fan,G., *et al.* (2014) Distribution, recognition and regulation of non-CpG methylation in the adult mammalian brain. *Nat. Neurosci.*, **17**, 215–222.
54. Olson,C.O., Pejhan,S., Kroft,D., Sheikholeslami,K., Fuss,D., Buist,M., Ali Sher,A., Del Bigio,M.R., Sztainberg,Y., Siu,V.M., *et al.* (2018) MECP2 mutation interrupts nucleolin-mTOR-P70S6K signaling in Rett syndrome patients. *Front. Genet.*, **9**, 635.
55. Pejhan,S., Del Bigio,M.R. and Rastegar,M. (2020) The MeCP2E1/E2-BDNF-miR132 homeostasis regulatory network is region-dependent in the human brain and is impaired in Rett syndrome patients. *Front. Cell Dev. Biol.*, **8**, 763.
56. Emanuele,N.V., Jurgens,J.K., Halloran,M.M., Tentler,J.J., Lawrence,A.M. and Kelley,M.R. (1992) The rat prolactin gene is expressed in brain tissue: detection of normal and alternatively spliced prolactin messenger RNA. *Mol. Endocrinol.*, **6**, 35–42.
57. Christman,J.K. (2002) 5-Azacytidine and 5-aza-2'-deoxycytidine as inhibitors of DNA methylation: mechanistic studies and their implications for cancer therapy. *Oncogene*, **21**, 5483–5495.
58. Christman,J.K., Mendelsohn,N., Herzog,D. and Schneiderman,N. (1983) Effect of 5-azacytidine on differentiation and DNA methylation in human promyelocytic leukemia cells (HL-60). *Cancer Res.*, **43**, 763–769.
59. Liu,L., Das,U., Ogunsola,S. and Xie,J. (2022) Transcriptome-Wide Detection of Intron/Exon Definition in the Endogenous Pre-mRNA Transcripts of Mammalian Cells and Its Regulation by Depolarization. *Int. J. Mol. Sci.*, **23**, 10157.
60. Toma,C., Hervas,A., Balmana,N., Vilella,E., Aguilera,F., Cusco,I., del Campo,M., Caballero,R., De Diego-Otero,Y., Ribases,M., *et al.* (2011) Association study of six candidate genes asymmetrically expressed in the two cerebral hemispheres suggests the involvement of BAIAP2 in autism. *J. Psychiatr. Res.*, **45**, 280–282.
61. Renbaum,P., Abrahamove,D., Fainsod,A., Wilson,G.G., Rottem,S. and Razin,A. (1990) Cloning, characterization, and expression in Escherichia coli of the gene coding for the CpG DNA methylase from Spiroplasma sp. strain MQ1(M.SssI). *Nucleic Acids Res.*, **18**, 1145–1152.
62. Marchler-Bauer,A., Bo,Y., Han,L., He,J., Lanczycki,C.J., Lu,S., Chitsaz,F., Derbyshire,M.K., Geer,R.C., Gonzales,N.R., *et al.* (2017) CDD/SPARCLE: functional classification of proteins via subfamily domain architectures. *Nucleic Acids Res.*, **45**, D200–D203.
63. Al-Mateen,M., Philippart,M. and Shields,W.D. (1986) Rett syndrome: a commonly overlooked progressive encephalopathy in girls. *Am. J. Dis. Child.*, **140**, 761–765.
64. Gold,W.A., Krishnarajy,R., Ellaway,C. and Christodoulou,J. (2018) Rett syndrome: a genetic update and clinical review focusing on comorbidities. *ACS Chem. Neurosci.*, **9**, 167–176.
65. Guerrini,R. and Parrini,E. (2012) Epilepsy in Rett syndrome, and CDKL5- and FOXG1-gene-related encephalopathies. *Epilepsia*, **53**, 2067–2078.
66. Moretti,P., Levenson,J.M., Battaglia,F., Atkinson,R., Teague,R., Antalffy,B., Armstrong,D., Arancio,O., Sweatt,J.D. and Zoghbi,H.Y. (2006) Learning and memory and synaptic plasticity are impaired in a mouse model of Rett syndrome. *J. Neurosci.*, **26**, 319–327.
67. Facchinetti,F., Zappella,M., Nalin,A., Petraglia,F., Bernasconi,S. and Genazzani,A.R. (1986) Plasma endorphins in Rett syndrome: preliminary data. *Am. J. Med. Genet. Suppl.*, **1**, 331–338.
68. Pepe,G., Stagi,S., Corica,D., Coco,R., Di Rosa,G., Bossowski,F., Skorupska,M., Aversa,T. and Wasniewska,M. (2023) In: *Hormone*

Research in Paeditrics. Karger Allschwilerstrasse 10, CH-4009 Basel, Switzerlannd. Vol. **96**, pp. 352–353.
69. Ghosh,R.P., Horowitz-Scherer,R.A., Nikitina,T., Gierasch,L.M. and Woodcock,C.L. (2008) Rett syndrome-causing mutations in human MeCP2 result in diverse structural changes that impact folding and DNA interactions. *J. Biol. Chem.*, **283**, 20523–20534.
70. Fu,X.D. and Ares,M. Jr (2014) Context-dependent control of alternative splicing by RNA-binding proteins. *Nat. Rev. Genet.*, **15**, 689–701.

Received: February 20, 2024. **Revised:** April 3, 2024. **Editorial Decision:** April 5, 2024. **Accepted:** April 14, 2024